Online-Journals.org

iJOE International Journal of Online and Biomedical Engineering

iJOE | eISSN: 2626-8493 | Vol. 20 No. 12 (2024) | OPEN ACCESS

https://doi.org/10.3991/ijoe.v20i12.49159

PAPER

Adaptive Control Using Radial Basis Function Neural Networks for Pneumatic Artificial Muscle Systems

Minh-Duc Duong, Viet-Thanh Nguyen, Quy-Thinh Dao(✉)

Hanoi University of Science and Technology, Hanoi, Vietnam

thinh.daoquy@hust.edu.vn

ABSTRACT

This study introduces a novel adaptive controller employing neural networks, particularly radial basis function (RBF) algorithms, to enhance the control performance of pneumatic artificial muscle (PAM)-based systems. The proposed controller seeks to address the nonlinearities and hysteresis inherent in PAM-based systems by integrating neural approximation. Experimental testing and comparisons with conventional controllers are conducted using an antagonistic configuration of PAMs. The results illustrate the precision and reliability of the proposed controller, suggesting potential for future advancements in trajectory tracking control of PAM-based systems.

KEYWORDS

pneumatic artificial muscle (PAM), radial-basis-function neural network (RBFNN), neural approximation, adaptive control

1 INTRODUCTION

Pneumatic artificial muscles (PAMs) are a type of soft actuator that has been widely used in biorobot [1, 2], medical device applications [3–5], and industrial [6, 7] due to their unique advantages. The most notable advantage of PAMs is their high power-to-weight ratio, which allows them to generate large forces while remaining lightweight. Additionally, PAMs are soft and flexible, allowing for safe human-robot interaction and stable motion speed. PAMs can also adapt to different loads, providing adaptable compliance. Furthermore, PAMs possess properties similar to those of human muscle, making them suitable for bio robotic applications that imitate the morphology and physiology of humans. Another advantage is that it is relatively low-cost to fabricate and easy to manufacture. Due to these advantages, PAMs have been widely used in rehabilitation systems where precision, adaptability, and human-like behavior are needed.

Despite the many advantages of PAMs, several disadvantages make modeling and controlling them difficult. One of the main disadvantages of PAMs is their

Duong, M.-D., Nguyen, V.-T., Dao, Q.-T. (2024). Adaptive Control Using Radial Basis Function Neural Networks for Pneumatic Artificial Muscle Systems. *International Journal of Online and Biomedical Engineering (iJOE)*, 20(12), pp. 109–123. https://doi.org/10.3991/ijoe.v20i12.49159

Article submitted 2024-03-17. Revision uploaded 2024-07-05. Final acceptance 2024-07-05.

nonlinearity, making it difficult to model their behavior accurately. Additionally, PAMs exhibit hysteresis, a non-ideal behavior resulting in a lag pertaining to the system's input and output. Another major disadvantage is the uncertainty of the model parameters, which makes it difficult to design controllers that can adapt to different conditions. Therefore, despite the many advantages of PAMs, the difficulties in modeling and controlling them have been a significant obstacle to their widespread use in practical applications.

Despite the difficulties in modeling and controlling PAMs, various control methods have been developed to overcome these challenges and achieve high performance in PAM control. The classical proportional integral derivative (PID) controller and its developed versions quickly became prevalent in various research domains. Based on PID control theory, research [8] presented a position control method for an artificial muscle that only used one pressure sensor. A pioneering PID-based controller, as presented in [9], is introduced to improve tracking performance and minimize hysteresis. Nevertheless, these PID controllers are only suitable for testing the mechanical structure and basic tracking ability of low-quality artificial muscle systems.

It is acknowledged that uncertainties and disturbances of pneumatic actuators like PAMs can be effectively solved by sliding mode control (SMC) and its enhanced version [10–14]. In addition, it essentially designs the controller in the discrete-time domain to apply it to digital controllers. For those reasons, several studies on discrete-time SMC have been conducted within the literature, focusing on various PAM-based systems, including investigations of equivalent control methodologies [15, 16] and reaching-law-based approaches [17, 18]. However, the chattering phenomenon is a major issue with any version of SMC specified in PAM-based actuators when tracking low-frequency trajectories.

Active disturbance rejection control (ADRC) methods have been considered to deal with the inherent uncertainties and disturbances of PAM-based systems. The fundamental idea of ADRC is to first consider the plant as a linear system and then use an extended state observer to estimate and reject the ignored dynamics and external disturbances as total disturbances. This approach does not require extensive knowledge of the system model or its disturbances, making it a useful controller for many applications. Both linear and nonlinear ADRCs have been used in literature [19–21]. However, research focusing on the practical aspects of the nonlinear ADRC scheme has been limited.

Artificial intelligence (AI) is widely used in various fields [22–24], including biomedical engineering [25–28]. Among AI techniques, fuzzy control, genetic algorithms, and neural networks are commonly employed in the development of intelligent control systems, showcasing their effectiveness over traditional control methods [29–31]. The use of fuzzy logic with conventional controllers, such as fuzzy-PID [32, 33] and fuzzy-SMC [34–36], has been widely implemented and achieved good results in the past, but these solutions are not flexible enough for many different application cases. As a result, learning algorithms tailored for fuzzy systems facilitate adaptive tuning of the system's parameters according to the provided signal patterns. Adaptive control is another approach we examine, which is employed by a controller that must adapt to a controlled system with variable or originally unclear characteristics [37]. The radial-basis-function neural network (RBFNN) is a popular choice among fuzzy logic neural networks and has been successfully used in various applications. Due to its capability to approximate uncertainty in complex model-uncertain systems with unidentified functions, it is viewed as a highly

effective solution for addressing diverse control challenges, notably dynamic uncertainty [38]. Many neural network controllers are used with adaptive control techniques for nonlinear systems to achieve high-precision performance [39–41]. With the outstanding capabilities mentioned above of RBFNN, which have the potential to mitigate the shortcomings of conventional controllers, we propose utilizing RBFNN to develop an adaptive controller aimed at enhancing control quality for the PAM system. This study employs indirect adaptive control methodologies, utilizing estimated parameters to calculate the essential controller parameters [42]. Additionally, we integrate the power of the RBF neural network to estimate uncertain elements in the system.

In summary, this paper presents several noteworthy contributions. Firstly, it introduces an adaptive controller, custom-designed to effectively handle antagonistic configurations of PAMs through neural approximation techniques. Secondly, the utilization of RBF algorithms is showcased to accurately approximate system uncertainties and determine the necessary controller parameters. Lastly, the practicality and potential impact of the proposed method are substantiated through experimental results conducted under diverse conditions. These results collectively underscore the effectiveness and suitability of the presented approach in the context of rehabilitation applications.

2 SYSTEM MODELING

A full representation of the pneumatic experimental platform is depicted in Figure 1. In the working object, a pair of PAMs is configured in an antagonistic arrangement. The structure dimensions are 25 mm in diameter and 400 mm in nominal length. The control valves (SMC, ITV2030-212S-X26) change and measure the pressure inside both PAMs. When there exists a pressure differential between the two PAMs, causing the pulley wheel to rotate, we employ a potentiometer (model WDD35D8T) to measure and record the resulting angle. This information is then sent to an embedded controller, specifically the MyRIO 1900 manufactured by National Instruments. This allows us to perform system adjustments via the computer.

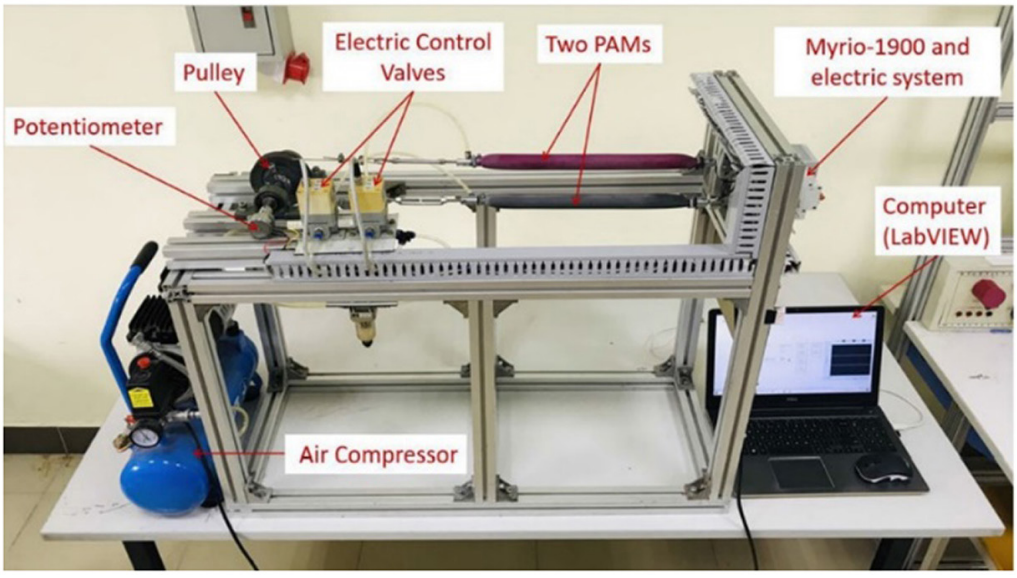

Fig. 1. The PAM-based actuator experimental platform

Due to the alignment in research focus, the mathematical model for the PAM-based system is derived from prior research conducted in our laboratory [18].

$$\ddot{x}(t) = \beta_2 \dot{x}(t) + \beta_1 x(t) + \alpha_1 u + \alpha_0 \tag{1}$$

where x is the chosen manipulated variable of the deviation angle, and u is the voltage control signal, which expresses the pressure change in PAMs. The parameters are described as follows:

$$\begin{cases} \alpha_1 = \dfrac{\left[2F_1 - 2K_1 L_0 - R\dot{\theta}(B_{1e} - B_{1f})\right]R}{J} \\ \alpha_0 = \dfrac{(F_1 P_{AP} - K_1 P_{AP} L_0)R}{J} \\ \beta_1 = \dfrac{-(2K_0 + 2K_1 P + K_1 P_{AP})R^2}{J} \\ \beta_2 = \dfrac{-\left[B_{0e} + B_{0f} + (B_{1e} + B_{1f})P_0 + B_{1e} P_{AP})\right]R^2}{J} \end{cases}$$

where R and J are the pulley's radius and inertia moment; L_0 and P_0 are the initial value of upper PAM's length and pressure; PAP is the initial different pressure of both PAMs; K_i and $F_i (i = 0,1)$ represent the spring and contractile elements of PAM's model; B_{ie} and B_{if} are the components of the PAM's damping coefficient. The notations e and f signify inflation and deflation of the muscle, respectively. For a more detailed understanding of the mathematical model of a single PAM, please consult the report [11].

The mathematical model's identified parameters α_0, α_1, β_1, β_2 are synthesized in Table 1.

Table 1. Identified model parameters

Parameters	α_0	α_1	β_1	β_2
Value	205	18.01	–4.83	7.35×10^{-4}

3 CONTROL DESIGN

The objective of this study is to introduce an adaptive controller utilizing online RBF neural approximation. This approach aims to enhance control precision and adjust to variations in parameters. The development of the adaptive law was grounded in the principles of Lyapunov stability theory, ensuring the attainment of stable closed-loop systems. Figure 2 provides a visual representation of the block diagram for the envisioned closed-loop neural-based control system, demonstrating the integration of the RBFNN in generating the control signal. The variable y represents the recorded angle, while y_d corresponds to the intended or reference signal. Due to the closed-loop control arrangement, the tracking error is fed back to both the controller and the adaptive mechanism, which includes the RBFNN. Within the adaptive cluster, the function $f(\boldsymbol{x})$, with uncertainties, undergoes approximation before being transmitted to the controller. The control output u is directed toward two control valves, thereby altering the pressures P_1 and P_2 of the two PAMs arranged antagonistically.

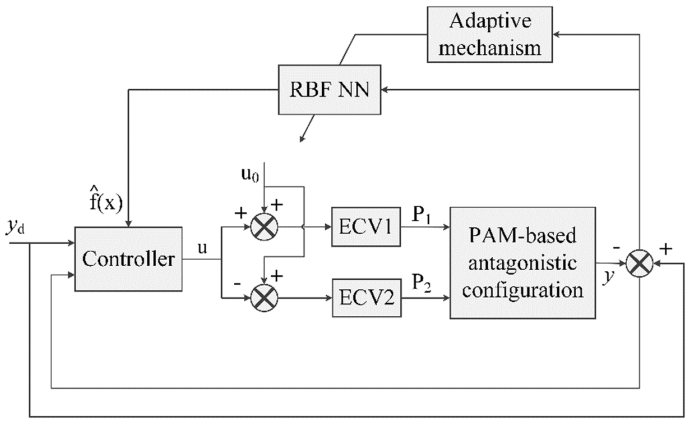

Fig. 2. System schematic of the proposed controller

A system with two PAMs arranged in an antagonistic configuration represents a single input, single output system. To facilitate the construction of the control algorithm, according to mathematical model (1), we described the PAM system in the controllable canonical form:

$$\begin{cases} \ddot{x} = f(x, \dot{x}) + gu \\ y = x \end{cases} \tag{2}$$

Where, $g = \alpha_1$ is a known function as a result of the identification process, while $f(x, \dot{x}) = \beta_2 \dot{x}(t) + \beta_1 x(t) + \alpha_0$ is an unknown nonlinear function.

Assume that y_d is the desired position signal. Declare e, vector $\boldsymbol{X}$, and vector $\boldsymbol{E}$ indicate the tracking errors, the vector of the system's states, and the vector of errors' states:

$$e = y_d - y,\ \boldsymbol{X} = [x\ \dot{x}]^T,\ \boldsymbol{E} = [e\ \dot{e}]^T$$

From (2), the inverse-based control algorithm can be developed as follows:

$$u^* = \frac{1}{g}[-f(\boldsymbol{X}) + \ddot{y}_d + \boldsymbol{K}^T \boldsymbol{E}] \tag{3}$$

Where, $\boldsymbol{K} = [k_p, k_d]^T$ is controller coefficient vector. Substituting equation (3) into equation (2), we obtain the closed-loop system as follows:

$$\ddot{e} + k_d \dot{e} + k_p e = 0 \tag{4}$$

To ensure the stability of the system and accurate output tracking, the polynomial $s^2 + k_d s + k_p = 0$ must be Hurwitz. Therefore, the selection of $\boldsymbol{K}$ is made to ensure that all the roots of the polynomial function lie to the left of the imaginary axis on the complex plane. However, it is realized that the controller (3) depends on an unknown factor $f(\boldsymbol{X})$. Thus, in the next subsection, we will employ the RBFNN to estimate $f(\boldsymbol{X})$.

3.1 Designing radial basis function neural networks

In this subsection, an RBFNN is selected to approximate the unknown components of the PAM-based system. Figure 3 illustrates the RBF neural network's architecture,

which comprises three layers, that has been proposed. For a more thorough explanation, the neural network takes two input nodes to represent the tracking error and its derivative. The hidden layer comprises m nodes, responsible for capturing the signal range and computing the weight vector. The output layer has only one node to present the approximated values. Specifically, $\boldsymbol{Z} = [z_1 \quad z_2]^T$ is the input vector, $\boldsymbol{h}(\boldsymbol{Z}) = [h_j]^T$ is the output of the hidden layer, and the specific values of each h_j are the values of the Gaussian functions for jth node in that layer:

$$h_j = exp\left(-\frac{\|\boldsymbol{Z} - \boldsymbol{c}_j\|^2}{b_j^2}\right) \tag{5}$$

Where, $\boldsymbol{c_j} = [c_{1j} \quad c_{2j}]^T$ denotes the central coordinate value of the jth node, and b_j represents the width value of the Gaussian function for the jth node with $j = 1, 2, \ldots, m$. The approximation $\hat{f}(\boldsymbol{X})$ of the uncertain element $f(\boldsymbol{X})$ of the system serves as the expected output. The output of the neural network is:

$$\hat{f}(\boldsymbol{X}) = \boldsymbol{W^T h}(\boldsymbol{Z}) = \sum_{j=1}^{m} W_j h_j \tag{6}$$

Where, $\boldsymbol{W} = [w_1, w_2, \ldots, w_m]^T$ is the weight vector.

Given the nature of RBF neural networks may be utilized to estimate uncertainties in control systems, in [38], the RBF neural network's input vector is chosen as the tracking error and the rate of change of it, that is, $\boldsymbol{Z} = \boldsymbol{E} = [e \ \dot{e}]^T$, the equation for utilizing the RBF algorithm to approximate $f(\boldsymbol{X})$ is outlined below:

$$\hat{f}(\boldsymbol{X}) = \widehat{\boldsymbol{W}}^T h(\boldsymbol{E}) \tag{7}$$

Where, $\widehat{\boldsymbol{W}}$ represents the calculated weight vector, subject to potential adjustments through the adaptive technique, and $h(\boldsymbol{E})$ is a Gaussian function.

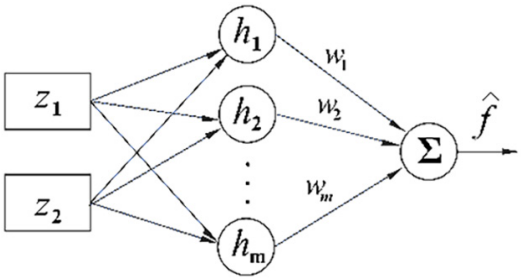

Fig. 3. RBF neural network structure

3.2 Designing control law

The RBF neural network has represented the uncertain nonlinear factor $f(\boldsymbol{X})$ from the previous section. As a result, the control law is fully defined:

$$u = \frac{1}{g}[-\hat{f}(\boldsymbol{X}) + \ddot{y}_d + \boldsymbol{K}^T \boldsymbol{E}] \tag{8}$$

Where, $\hat{f}(\boldsymbol{X})$ is the approximated parameter for $f(\boldsymbol{X})$.

3.3 Designing adaptive law

In this section, the adaptive law is derived using the Lyapunov stability approach to approximate $f(\boldsymbol{X})$ with $\hat{f}(\boldsymbol{X})$ while maintaining the stability of the system. As indicated in equation (7), the approximation $\hat{f}(\boldsymbol{X})$ is achieved through a radial basis function (RBF) neural network. Consequently, the updating rule for $\widehat{\boldsymbol{W}}$ will be formulated. By substituting the control law (8) into equation (2), the closed-loop system is expressed as:

$$\ddot{e} = -\boldsymbol{K}^T \boldsymbol{E} + [\hat{f}(\boldsymbol{X}) - f(\boldsymbol{X})] \tag{9}$$

To facilitate a more convenient transformation, we define two new matrices:

$$\boldsymbol{\Lambda} = \begin{bmatrix} 0 & 1 \\ -k_p & -k_d \end{bmatrix}, \boldsymbol{B} = \begin{bmatrix} 0 \\ 1 \end{bmatrix} \tag{10}$$

Equation (9) can be rewritten as follows:

$$\dot{\boldsymbol{E}} = \boldsymbol{\Lambda E} + \boldsymbol{B}[\hat{f}(\boldsymbol{X}) - f(\boldsymbol{X})] \tag{11}$$

Supposing that $f(\boldsymbol{X})$ can be calculated by an ideal RBF neural network with ideal weight values $\boldsymbol{W}^* = \left[w_1^*, w_2^*, \ldots, w_m^*\right]^T$:

$$f(\boldsymbol{X}) = \boldsymbol{W}^{*T} h(\boldsymbol{E}) \tag{12}$$

Then equation (11) becomes:

$$\dot{\boldsymbol{E}} = \boldsymbol{\Lambda E} + \boldsymbol{B}(\widehat{\boldsymbol{W}} - \boldsymbol{W}^*)^T h(\boldsymbol{E}) \tag{13}$$

Considering the following Lyapunov function:

$$V = \frac{1}{2}\boldsymbol{E}^T \boldsymbol{P E} + \frac{1}{2\gamma}(\widehat{\boldsymbol{W}} - \boldsymbol{W}^*)^T (\widehat{\boldsymbol{W}} - \boldsymbol{W}^*) \tag{14}$$

Where, γ is a positive numerical value, $\widehat{\boldsymbol{W}} - \boldsymbol{W}^*$ signifies the error in parameter estimation, and $\boldsymbol{P}$ is a symmetric and positive definite matrix that fulfills the Lyapunov equation:

$$\boldsymbol{\Lambda}^T \boldsymbol{P} + \boldsymbol{P\Lambda} = -\boldsymbol{Q} \tag{15}$$

Where, $\boldsymbol{Q}$ is an arbitrary 2×2 positive definite matrix and $\boldsymbol{\Lambda}$ is given by equation (10).

Differentiating equation (14) with respect to time, we have:

$$\dot{V} = \frac{1}{2}\dot{\boldsymbol{E}}^T \boldsymbol{P E} + \frac{1}{2}\boldsymbol{E}^T \boldsymbol{P}\dot{\boldsymbol{E}} + \frac{1}{\gamma}(\widehat{\boldsymbol{W}} - \boldsymbol{W}^*)^T \dot{\widehat{\boldsymbol{W}}} \tag{16}$$

By substituting equation (15) into equation (16), one can obtain

$$\dot{V} = -\frac{1}{2}\boldsymbol{E}^T \boldsymbol{Q E} + \frac{1}{\gamma}(\widehat{\boldsymbol{W}} - \boldsymbol{W}^*)^T [\dot{\widehat{\boldsymbol{W}}} + \gamma \boldsymbol{E}^T \boldsymbol{P B} h(\boldsymbol{E})] \tag{17}$$

Select the adaptation (weight updating) law as:

$$\dot{\widehat{\boldsymbol{W}}} = -\gamma \boldsymbol{E}^T \boldsymbol{P B} h(\boldsymbol{E}) \tag{18}$$

Then,

$$\dot{V} = -\frac{1}{2}\boldsymbol{E}^T\boldsymbol{Q}\boldsymbol{E} \leq 0 \tag{19}$$

The system is stable in the sense of Lyapunov.

4 EXPERIMENTAL RESULTS

A variety of situations are tested with different trajectories to evaluate the performance of the recommended controller. Experiments are carried out in both cases, without and with loads. The sampling cycle T_s is set at 5 ms throughout each experimental case.

Acknowledging the intricate characteristics of the artificial neural system, we have opted for a particular setup, specifically a 2-5-1 RBFNN. The neural network's input is composed of two nodes, which represent both the tracking error and its rate of change in control. The hidden layer, identified as h_j, comprises five nodes meticulously selected to encompass the full signal range and facilitate efficient computation of weight vectors. Careful consideration has been given to selecting values for b_j to guarantee optimal performance. Finally, the output layer consists of a single node that signifies the estimated parameter of the pneumatic muscle actuator, denoted as $f(\boldsymbol{X})$.

RBFNN approximation requires careful selection of the parameters $\boldsymbol{c}_j$ and b_j to ensure that the Gaussian function is effectively mapped to the input values. If these parameters are not chosen appropriately, the RBF network may not be valid. To avoid this, it is recommended to set the initial values of $\boldsymbol{c}_j$ and b_j within the range of the input values for the RBF network. This way, only the weight value needs to be updated while $\boldsymbol{c}_j$ and b_j remain fixed. The initial weight value is set to zero, and the parameters $\boldsymbol{c}_j$ and b_j are designed as $[c_j] = \begin{bmatrix} 10 & 5 & 0 & -5 & -10 \\ 20 & 10 & 0 & -10 & -20 \end{bmatrix}$, and $b_j = 2$.

During the system modeling process, the value of λ_0 was determined to be 18.01. Two parameters, k_p = 40, k_d = 0.1, are chosen according to the rule described in Section 3. Other parameters were fine-tuned through a meticulous adjustment process and finally chosen as follows: $\boldsymbol{Q} = \begin{bmatrix} 20 & 0 \\ 0 & 20 \end{bmatrix}$, and $\gamma = 120$.

Because of the likeness in control concepts and research subject matter, all experimental results will be compared with the meticulously studied fuzzy-PID controller (FPIDC) presented in the work in [43], where the PID controller's parameters are adjusted by fuzzy logic.

4.1 Tracking signals without loads

In the subsequent phase of the study, desired trajectories for evaluating the controller's performance are selected as sinusoidal signals with an amplitude of 40° and frequencies ranging from 0.2 Hz to 1.0 Hz. Triangular signals featuring identical amplitudes and frequencies of 0.2 Hz and 0.5 Hz are additionally employed as desired trajectories. These signals serve the purpose of assessing the controller's tracking performance and its ability to handle various input profiles. The experimental

results, corresponding to the aforementioned signal types, are depicted in Figures 4 and 5, respectively. Tracking performances are depicted in the upper sub-figures, where the measured trajectories are reflected by the dashed red lines of the FPIDC and the dashed blue lines of the adaptive RBFNN controller, compared to the green line representing the desired signals. Meanwhile, the tracking errors are shown in the lower sub-figures, and Table 2 provides the two controllers' root-mean-square tracking error (RMSE) values.

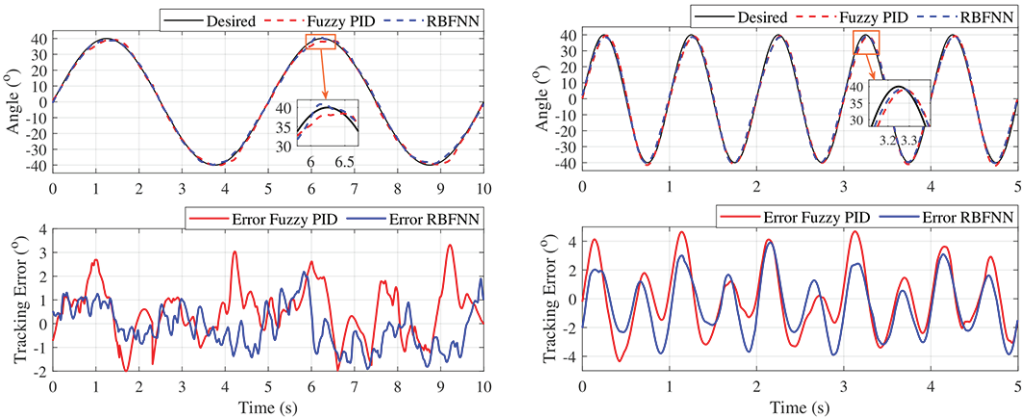

(a) 0.2 Hz (b) 1.0 Hz

Fig. 4. Experiment results when tracking sinusoidal trajectories

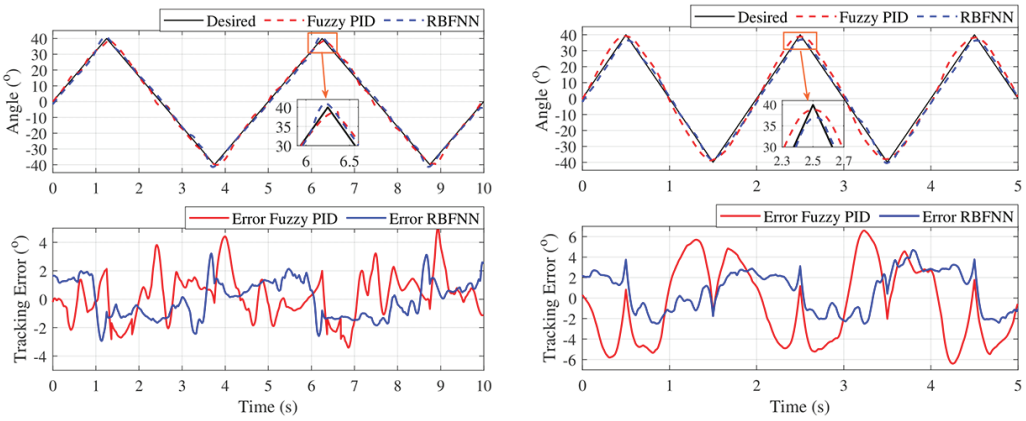

(a) 0.2 Hz (b) 0.5 Hz

Fig. 5. Experiment results for tracking triangular trajectories

It is evident from all the experimental outcomes that both the FPIDC and the adaptive RBFNN controller can track the desired signals effectively. But inspecting the steady-state errors and RMSE values deeply, we acknowledge that the RBFNN controller brings better performance, especially when the desired signals have a high frequency or are no longer smooth, like triangular ones. In the exclusive assessment of the RBFNN's performance, we observe a slight degradation in control performance with increasing trajectory frequency, although still achieving precise results. When following sine wave signals, the tracking errors are limited to approximately ± 2.0° at low frequencies and never exceed 4.0° at higher frequencies, which demonstrates commendable tracking performance.

For triangular trajectories, the results show slightly lower precision. However, it's worth noting that if the frequency exceeds 0.5 Hz, maintaining performance

becomes challenging, primarily due to the dynamic hysteresis and time-intensive response characteristics of the pneumatic artificial muscles.

Table 2. Quantitative evaluation of two controllers when tracking periodic signals

Frequency	Sinusoidal		Triangular	
	FPIDC	RBFNN	FPIDC	RBFNN
0.2 Hz	1.20	0.91	1.62	1.31
0.5 Hz	1.84	1.47	2.64	2.10
0.8 Hz	2.04	1.88	–	–
1.0 Hz	2.27	2.03	–	–

A gait pattern is also used as the desired signal to evaluate the application of PAM and the proposed controller in rehabilitation. The desired trajectories of hip and knee joints are programmed based on human movement data from the well-known textbook [44]. Two frequencies, 0.2 Hz and 0.5 Hz, of the desired signal are used for this experimental condition. Figure 6 shows the tracking performance of the RBFNN controller and its counterpart when tracking the 0.2 Hz gait-pattern trajectory.

We have a similar conclusion about the performance with two other types of desired trajectories: sine and triangle signals. Both controllers can track the desired signal, and the RBFNN-based one achieves better tracking with lower fluctuation than the fuzzy-PID one. The quantity evaluation of both controllers in this experiment is provided in Table 3. We can see that when tracking the hip trajectory, both controllers present worse performance with RMSE are 2.47° and 1.84° with 0.2 Hz of frequency. When the frequency increases to 0.5 Hz, these values are 3.27° and 2.28°. The reason is that there is a big gap between the measured and desired trajectories at the startup.

Table 3. Quantitative evaluation of two controllers when tracking gait pattern signals

Frequency	Hip Joint		Knee Joint	
	FPIDC	RBFNN	FPIDC	RBFNN
0.2 Hz	2.47	1.84	1.45	1.10
0.5 Hz	3.27	2.28	2.84	1.66

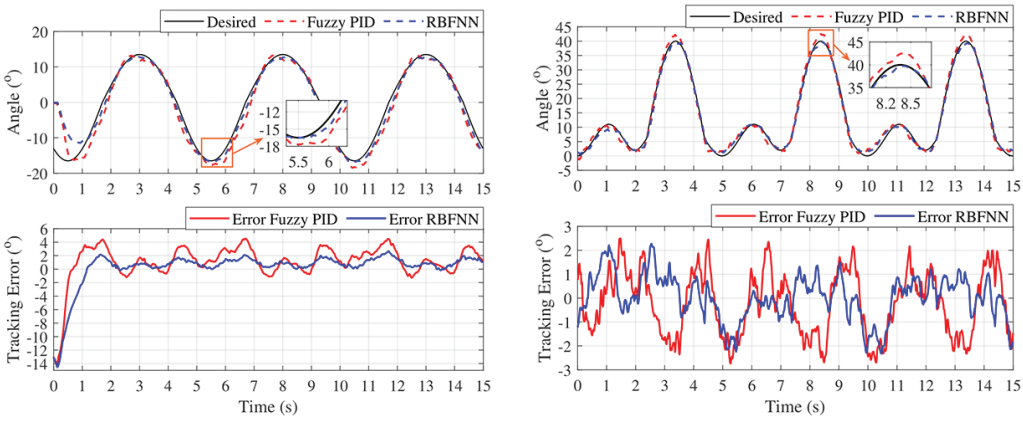

(a) Hip Trajectory **(b) Knee Trajectory**

Fig. 6. Experiment results when tracking human movement's trajectories

4.2 Tracking signals with loads

To assess the robustness of the proposed control approach, additional loads are abruptly introduced to the system upon reaching the steady state. Loads of 3 kg and 5 kg are suspended by a rope and lifted by the operator. Subsequently, the system initially tracks a sinusoidal signal with an amplitude of 40° degrees and a frequency of 0.5 Hz. At the 4-second mark from the system reaching the steady state, the operator releases the load, introducing it as an external disturbance. The experimental results are visualized in Figure 7. It's noticeable that the tracking performance experiences fluctuations when the impact takes place. Eventually, both control strategies recover from this fluctuation. Despite similar overall results, the RBF neural network exhibits a faster return to the intended trajectory compared to the comparative strategy.

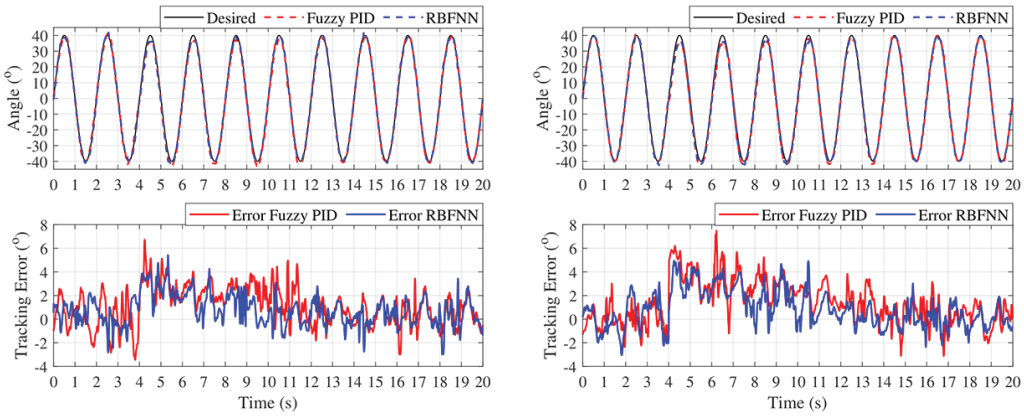

(a) Load m = 3 kg **(b) Load m = 5 kg**

Fig. 7. Experiment results for tracking a 40° amplitude and 0.5 Hz frequency sinusoidal trajectory with a load

The change in the applied weight notably impacts the performance, which directly affects the system. As weight increases, achieving an optimal tracking trajectory becomes more challenging and time-consuming. With a 3 kg load, it takes approximately 6.0 seconds to restore the desired stability, while a heavier load requires 8.0 seconds (equivalent to 3 and 4 cycles within this 0.5 Hz frequency experimental setting). The experimental results align with the rehabilitation criteria established for the commercial LOKOMAT system [45]. The above evaluations are proved in graphs, and the RMSE values are shown in Table 4.

Table 4. Quantitative evaluation of two controllers when tracking gait pattern signals

Load Weight	RMSE	
	FPIDC	RBFNN
3 kg	1.94	1.51
5 kg	2.27	1.77

5 CONCLUSION

This study introduces an adaptive controller utilizing RBFNN approximation for an antagonistic configuration of two pneumatic artificial muscles. The integration of

an RBF neural network in the design is aimed at effectively approximating unknown elements in the control law. This allows the proposed system to adapt to different rehabilitation subjects with the same performance without any manual adjustment. Additionally, the stability of the system and the adaptive law have been rigorously analyzed using Lyapunov's stability theory. The entire system operates seamlessly and efficiently as a cohesive unit.

In a comprehensive assessment, it is evident that the proposed controller generates adaptable control signals capable of accommodating a range of system conditions while consistently achieving outstanding tracking performance. For example, during the tracking of sinusoidal signals with a load-free scenario and an amplitude of 40.0°, the tracking error consistently stays below 4.0° (equivalent to 10% of the amplitude), irrespective of the signal frequency.

Adding loads to the system is a more realistic circumstance, which indicates that the controller's performance is still guaranteed to adhere to LOKOMAT's accuracy, as specified in the reference [45]. This promises to be able to build a complete rehabilitation robot for both the lower and upper limbs of patients. Taking a deeper look inside, the foundation ideas of the control algorithm led to some specific upper hands. The process by which RBF updates the parameters for control signals can curtail the effects of unstable elements. Adaptability and stability are proven in transient-impact situations as well. Whereas dynamic hysteresis and slow response are inherent weaknesses that need further study. In the future developments outlined in this paper, our intentions include integrating more advanced RBF algorithms with other sophisticated control strategies, leveraging the versatile capabilities of neural networks. Furthermore, we intend to conduct a series of practical experiments to serve rehabilitation purposes.

6 REFERENCES

[1] F. Escobar, S. Díaz, C. Gutiérrez, Y. Ledeneva, C. Hernández, D. Rodríguez, and R. Lemus, "Simulation of control of a scara robot actuated by pneumatic artificial muscles using rnapm," *Journal of Applied Research and Technology*, vol. 12, no. 5, 2014. https://doi.org/10.1016/S1665-6423(14)70600-5

[2] A. Rezoug, B. Tondu, and M. Hamerlain, "Experimental study of nonsingular terminal sliding mode controller for robot arm actuated by pneumatic artificial muscles," *IFAC Proceedings Volumes*, vol. 47, no. 3, pp. 10113–10118, 2014. https://doi.org/10.3182/20140824-6-ZA-1003.00730

[3] S. K. Banala, S. H. Kim, S. K. Agrawal, and J. P. Scholz, "Robot assisted gait training with active leg exoskeleton (alex)," in *2008 2nd IEEE RAS & EMBS International Conference on Biomedical Robotics and Biomechatronics*, Scottsdale, AZ, USA, 2008, pp. 653–658. https://doi.org/10.1109/BIOROB.2008.4762885

[4] K. Kadota, M. Akai, K. Kawashima, and T. Kagawa, "Development of a power-assist robot arm using pneumatic rubber muscles with a balloon sensor," in *RO-MAN 2009- The 18th IEEE International Symposium on Robot and Human Interactive Communication*, 2009, pp. 546–551. https://doi.org/10.1109/ROMAN.2009.5326335

[5] A. D. D. R. Carvalho, N. Karanth P, and V. Desai, "Characterization of pneumatic muscle actuators and their implementation on an elbow exoskeleton with a novel hinge design," *Sensors and Actuators Reports*, vol. 4, p. 100109, 2022. https://doi.org/10.1016/j.snr.2022.100109

[6] K. Deckers, P. Guillaume, D. Lefeber, G. De Roeck, and E. Reynders, "Modal testing of bridges using low-weight pneumatic artificial muscle actuators," in *Proceedings of IMAC 26, the International Modal Analysis Conference*, 2008.

[7] J. Radojicic, D. Surdilovic, and G. Schreck, "Modular hybrid robots for safe human-robot interaction," *Zenodo*, 2009. https://doi.org/10.5281/zenodo.1077433

[8] K. Yokoyama and K. Kogiso, "Pid position control of McKibben pneumatic artificial muscle using only pressure feedback," in *2018 Annual American Control Conference (ACC)*, 2018, pp. 3362–3367. https://doi.org/10.23919/ACC.2018.8431631

[9] G. Andrikopoulos, G. Nikolakopoulos, and S. Manesis, "Advanced nonlinear pid-based antagonistic control for pneumatic muscle actuators," *IEEE Transactions on Industrial Electronics*, vol. 61, no. 12, pp. 6926–6937, 2014. https://doi.org/10.1109/TIE.2014.2316255

[10] J. Lilly and P. Quesada, "A two-input sliding-mode controller for a planar arm actuated by four pneumatic muscle groups," *IEEE Transactions on Neural Systems and Rehabilitation Engineering*, vol. 12, no. 3, pp. 349–359, 2004. https://doi.org/10.1109/TNSRE.2004.831490

[11] K. Xing, J. Huang, Y. Wang, J. Wu, and Q. X. J. He, "Tracking control of pneumatic artificial muscle actuators based on sliding mode and nonlinear disturbance observer," *IET Control Theory & Applications*, vol. 4, no. 10, pp. 2058–2070, 2010. https://doi.org/10.1049/iet-cta.2009.0555

[12] C.-J. Chiang and Y.-C. Chen, "Neural network fuzzy sliding mode control of pneumatic muscle actuators," *Engineering Applications of Artificial Intelligence*, vol. 65, pp. 68–86, 2017. https://doi.org/10.1016/j.engappai.2017.06.021

[13] C. P. Vo, X. D. To, and K. K. Ahn, "A novel adaptive gain integral terminal sliding mode control scheme of a pneumatic artificial muscle system with time-delay estimation," *IEEE Access*, vol. 7, pp. 141133–141143, 2019. https://doi.org/10.1109/ACCESS.2019.2944197

[14] J. Mohorcic and L. Dong, "Extended state observer-based pressure control for pneumatic actuator servo systems," *Control Theory and Technology*, vol. 19, pp. 64–79, 2021. https://doi.org/10.1007/s11768-021-00038-y

[15] Q.-T. Dao, M.-L. Nguyen, and S.-I. Yamamoto, "Discrete-time fractional order integral sliding mode control of an antagonistic actuator driven by pneumatic artificial muscles," *Applied Sciences*, vol. 9, no. 12, p. 2503, 2019. https://doi.org/10.3390/app9122503

[16] Q.-T. Dao, D.-H. Mai, D. K. Nguyen, and N. T. Ly, "Adaptive parameter integral sliding mode control of pneumatic artificial muscles in antagonistic configuration," *Journal of Control, Automation, and Electrical Systems*, vol. 33, p. 1116–1124, 2022. https://doi.org/10.1007/s40313-022-00902-5

[17] R. Fellag, M. Hamerlain, S. Laghrouche, and N. Achour, "Adaptive discrete sliding mode control of a pneumatic artificial muscle robot," in *2017 5th International Conference on Electrical Engineering-Boumerdes (ICEE-B)*, 2017, pp. 1–6. https://doi.org/10.1109/ICEE-B.2017.8192099

[18] Q.-T. Dao, T.-K. Le Tri, V.-A. Nguyen, and M.-L. Nguyen, "Discrete time sliding mode control with power rate exponential reaching law of a pneumatic artificial muscle system," *Control Theory and Technology*, vol. 20, pp. 514–524, 2022. https://doi.org/10.1007/s11768-022-00117-8

[19] L. Zhao, X. Liu, and T. Wang, "Trajectory tracking control for double joint manipulator systems driven by pneumatic artificial muscles based on a nonlinear extended state observer," *Mechanical Systems and Signal Processing*, vol. 122, pp. 307–320, 2019. https://doi.org/10.1016/j.ymssp.2018.12.016

[20] S. Wang, W. Tan, and D. Li, "Design of linear adrc for load frequency control of power systems with wind turbines," in *2016 14th International Conference on Control, Automation, Robotics, and Vision (ICARCV)*, 2016, pp. 1–5. https://doi.org/10.1109/ICARCV.2016.7838795

[21] S. Aole, I. Elamvazuthi, L. Waghmare, B. Patre, and F. Meriaudeau, "Improved active disturbance rejection control for trajectory tracking control of lower limb robotic rehabilitation exoskeleton," *Applied Sciences*, vol. 20, no. 13, p. 1287, 2020. https://doi.org/10.3390/app12031287

[22] M. A. Alsharaiah, "Neural network prediction model to explore complex nonlinear behavior in dynamic biological network," *Int. J. Interact. Mob. Technol. (iJIM)*, vol. 16, no. 12, pp. 32–51, 2022. https://doi.org/10.3991/ijim.v16i12.30467

[23] T. Ganokratanaa and M. Ketcham, "An intelligent autonomous document mobile delivery robot using deep learning," *Int. J. Interact. Mob. Technol. (iJIM)*, vol. 16, no. 21, pp. 4–22, 2022. https://doi.org/10.3991/ijim.v16i21.32071

[24] H. A. Abu-Alsaad, "CNN-based smart parking system," *Int. J. Interact. Mob. Technol. (iJIM)*, vol. 17, no. 11, pp. 155–170, 2023. https://doi.org/10.3991/ijim.v17i11.37033

[25] O. M. Al-hazaimeh, A. Abu-Ein, N. Tahat, M. Al-Smadi, and M. Al-Nawashi, "Combining artificial intelligence and image processing for diagnosing diabetic retinopathy in retinal fundus images," *Int. J. Onl. Eng. (iJOE),* vol. 18, no. 13, pp. 131–151, 2022. https://doi.org/10.3991/ijoe.v18i13.33985

[26] N. Gharaibeh, A. Abu-Ein, O. M. Al-hazaimeh, K. M. Nahar, W. A. Abu-Ain, and M. Al-Nawashi, "Swin transformer-based segmentation and multi-scale feature pyramid fusion module for Alzheimer's disease with machine learning," *Int. J. Onl. Eng. (iJOE),* vol. 19, no. 4, pp. 22–50, 2023. https://doi.org/10.3991/ijoe.v19i04.37677

[27] M. Kh. Khazaaleh *et al.*, "Handling DNA malfunctions by an unsupervised machine learning model," *Journal of Pathology Informatics*, vol. 14, p. 100340, 2023. https://doi.org/10.1016/j.jpi.2023.100340

[28] O. M. Al-Hazaimeh, M. Al-Nawashi, and M. Saraee, "Geometrical-based approach for robust human image detection," *Multimed. Tools Appl.*, vol. 78, pp. 7029–7053, 2019. https://doi.org/10.1007/s11042-018-6401-y

[29] P. Gupta and N. K. Sinha, "Intelligent control of robotic manipulators: Experimental study using neural networks," *Mechatronics*, vol. 10, nos. 1–2, pp. 289–305, 2000. https://doi.org/10.1016/S0957-4158(99)00059-8

[30] G. Naganna and S. Kumar, "Conventional and intelligent controllers for robotic manipulators," in *2006 IEEE International Conference on Industrial Technology*, 2006, pp. 424–428. https://doi.org/10.1109/ICIT.2006.372240

[31] Zaitceva, Iuliia, and B. Andrievsky, "Methods of intelligent control in mechatronics and robotic engineering: A survey," *Electronics*, vol. 11, no. 15, p. 22443, 2022. https://doi.org/10.3390/electronics11152443

[32] S. Chan, J. Lilly, D. Repperger, and J. Berlin, "Fuzzy PD+i learning control for a pneumatic muscle," in *the 12th IEEE International Conference on Fuzzy Systems, 2003, FUZZ '03*, 2003, vol. 1, pp. 278–283. https://doi.org/10.1109/FUZZ.2003.1209375

[33] H. P. H. Anh and K. K. Ahn, "Hybrid control of a pneumatic artificial muscle (pam) robot arm using an inverse narx fuzzy model," *Engineering Applications of Artificial Intelligence*, vol. 24, no. 4, pp. 697–716, 2011. https://doi.org/10.1016/j.engappai.2010.11.007

[34] C. V. Kien, T. T. Huan, D. T. Thai, and H. P. H. Anh, "Implementation of adaptive fuzzy sliding mode control for nonlinear uncertain serial pneumatic-artificial-muscle (PAM) robot system," in *2017 International Conference on System Science and Engineering (ICSSE)*, 2017, pp. 83–88. https://doi.org/10.1109/ICSSE.2017.8030842

[35] D. Liang, N. Sun, Y. Wu, G. Liu, and Y. Fang, "Fuzzy-sliding mode control for humanoid arm robots actuated by pneumatic artificial muscles with unidirectional inputs, saturations, and dead zones," *IEEE Transactions on Industrial Informatics*, vol. 18, no. 5, pp. 3011–3021, 2022. https://doi.org/10.1109/TII.2021.3111655

[36] A. Rezoug, S. Boudoua, and F. Hamerlain, "Application of fuzzy sliding mode to control of manipulator robots actuated by pneumatic artificial muscles," *IFAC Proceedings Volumes*, vol. 42, no. 19, pp. 580–585, 2009. https://doi.org/10.3182/20090921-3-TR-3005.00099

[37] C. Cao, L. Ma, and Y. Xu, "Adaptive control theory and applications," *Journal of Control Science and Engineering*, vol. 2012, pp. 1–2, 2012. https://doi.org/10.1155/2012/827353

[38] J. Liu, *Radial Basis Function (RBF) Neural Network Control for Mechanical Systems*. 1st Edition. Berlin: Springer Berlin, Heidelberg, 2013. https://doi.org/10.1007/978-3-642-34816-7

[39] W. He, Y. Chen, and Z. Yin, "Adaptive neural network control of an uncertain robot with full-state constraints," *IEEE Transactions on Cybernetics*, vol. 46, no. 3, pp. 620–629, 2016. https://doi.org/10.1109/TCYB.2015.2411285

[40] W. He, Z. Yan, C. Sun, and Y. Chen, "Adaptive neural network control of a flapping wing microaerial vehicle with disturbance observer," *IEEE Transactions on Cybernetics*, vol. 47, no. 10, pp. 3452–3465, 2017. https://doi.org/10.1109/TCYB.2017.2720801

[41] H. Yang and J. Liu, "An adaptive RBF neural network control method for a class of non-linear systems," *IEEE/CAA Journal of Automatica Sinica*, vol. 5, no. 2, pp. 457–462, 2018. https://doi.org/10.1109/JAS.2017.7510820

[42] K. J. Astrom and B. Wittenmark, *Adaptive Control*, 2nd Edition, Addison Wesley, 1995.

[43] Q. T. Dao, D.-H. Mai, and D.-K. Nguyen, "Experimental validation for pneumatic artificial muscles using fuzzy PID control," *Measurement, Control, and Automation*, vol. 2, no. 1, pp. 58–64, 2022.

[44] D. A. Winter, *Biomechanics and Motor Control of Human Movement*, 4th Edition. John Wiley & Sons, Ltd, 2009. https://doi.org/10.1002/9780470549148

[45] R. Riener, L. Lunenburger, S. Jezernik, M. Anderschitz, G. Colombo, and V. Dietz, "Patient-cooperative strategies for robot-aided treadmill training: First experimental results," *IEEE Transactions on Neural Systems and Rehabilitation Engineering*, vol. 13, no. 3, pp. 380–394, 2005. https://doi.org/10.1109/TNSRE.2005.848628

7 AUTHORS

Minh-Duc Duong received his Ph.D. degree in Electronic and Information Engineering from Toyohashi University of Technology in 2008. Presently, he is an associate professor at the Department of Automation Engineering, School of Electrical and Electronic Engineering, Hanoi University of Science and Technology. His research interests include rehabilitation robots, vibration suppression control, and bilateral teleoperation robot systems.

Viet-Thanh Nguyen is a senior in the School of Electrical and Electronic Engineering at the Hanoi University of Science and Technology. As a member of the esteemed Talented Program in Automation and Control Engineering, Viet-Thanh started his research journey during his sophomore year at the Motion Control and Applied Robotics Laboratory (MoCAR). His main research orientation is advanced control algorithms for the pneumatic artificial muscle system (PAM) using (RBFNNs).

Quy-Thinh Dao received both his B.S. and M.S. degrees in Electrical Engineering from Hanoi University of Science and Technology, Vietnam, in 2007 and 2010, respectively. Subsequently, he completed his Ph.D. in functional control systems at Shibaura Institute of Technology, Tokyo, Japan, in 2019. Currently serving as a senior lecturer in the Department of Automation Engineering within the School of Electrical and Electronic Engineering at Hanoi University of Science and Technology, he specializes in captivating research areas such as smart actuators, control theory, and the advancement of welfare and service robotics (E-mail: thinh.daoquy@hust.edu.vn).